Annals of Glaciology

Article

Cite this article: Scanlan KM, Rutishauser A, Young DA, Blankenship DD (2020). Interferometric discrimination of cross-track bed clutter in ice-penetrating radar sounding data. *Annals of Glaciology* **61**(81), 68–73. https://doi.org/10.1017/aog.2020.20

Received: 1 December 2019
Revised: 9 April 2020
Accepted: 14 April 2020
First published online: 10 June 2020

Key words:
Clutter; interferometry; radar remote sensing; radioglaciology

Author for correspondence:
Kirk M. Scanlan,
E-mail: kirk.scanlan@utexas.edu

cambridge.org/aog

Interferometric discrimination of cross-track bed clutter in ice-penetrating radar sounding data

Kirk M. Scanlan, Anja Rutishauser, Duncan A. Young and Donald D. Blankenship

University of Texas Institute for Geophysics, University of Texas at Austin, Austin, TX, USA

Abstract

The interpretations of relevant interfaces (i.e. the surface and bed) in radar sounding datasets over glaciers and ice sheets are primary boundary conditions in a variety of climate studies and particularly subglacial water routing models. It is therefore necessary to ensure these interpretations are consistent and not affected by cross-track clutter. For the surface interface, interferometry and a family of methods relying on digital elevation models have been used to successfully discriminate cross-track surface clutter. Here we present how interferometry can be applied to the problem of basal clutter from cross-track bed topography. Our approach is based on a comparison of the differential phases of ambiguous reflectors that may represent bed clutter and the differential phase of a reflector in an adjacent area that appears unaffected by basal clutter. The reflector yielding the smallest interferometric phase difference relative to the unambiguous bed reflector is considered to represent its consistent continuation. We successfully demonstrate our approach using 60 MHz center frequency MARFA data collected over Devon Ice Cap in the Canadian Arctic. Finally, we investigate the effects of clutter-affected and interferometry-corrected bed interpretations on ice layer thickness estimates, basal hydraulic head gradients and the potential extent of inferred subglacial water bodies.

Introduction

For decades, radar sounding has been a method of choice in the large-scale characterization of ice sheets, ice caps and glaciers (de Robin, 1975; Bingham and Siegert, 2007). Not only can radar sounding measurements be qualitatively interpreted to yield estimates of the ice mass thicknesses and underlying bed topographies but the quantitative interpretation of radar bed echo strengths is used to characterize subglacial hydrology and identify bodies of subglacial liquid water (i.e. lakes) (Shabtaie and Bentley, 1988; Wright and Siegert, 2012; Young and others, 2016; Rutishauser and others, 2018). These interpretations provide critical boundary conditions for glacial dynamic and subglacial hydrology models as well as potential targets for extreme habitat microbiological studies.

In all studies relying on radar sounding data, it is important to define the reflectors chosen to represent particular horizons of interest (i.e. the surface, bed or englacial layers) consistently, which is complicated by the wide beam patterns associated with conventional dipole antennas (Peters and others, 2007). Coherent (magnitude and phase) acquisition systems and subsequent synthetic aperture radar (SAR) focusing can be used to improve along-track reflector resolution (Leuschen and others, 2000; Legarsky and others, 2001; Peters and others, 2005, 2007; Hélière and others, 2007), but the cross-track beam pattern remains broad. The end effect is a radar image (the radargram) that may contain anomalous signals reflected from cross-track off-nadir surface and subsurface features (i.e. clutter) that can be misinterpreted as a reflector of interest.

Several techniques have been proposed to discriminate surface cross-track clutter in airborne radar sounding data including radargram reprojection and cluttergram simulation (Holt and others, 2006) as well as interferometry (Castelletti and others, 2017; Haynes and others, 2018). Radargram reprojection involves the cross-track mapping of radargram energy onto a digital elevation model (DEM) as if it were all derived from surface scatterers. Surface clutter is then discriminated by comparing where the signal in the radargram would have been reflected from had it originated on the surface. Energy mapping to distinct topographic features on the surface can then be used to infer if that signal represents surface clutter. Discrimination through cluttergram simulation represents the opposite approach; whereby a DEM is used to simulate a radargram assuming no subsurface reflectors are present. Similar echo features in both the simulated cluttergram and the measured radargram are then likely to originate from surface reflectors. Finally, interferometry discriminates clutter by measuring the phase difference between an echo reflecting from the same surface feature but arriving at two antennas separated in the cross-track direction. Ignoring any systematic phase offset between the antennas due to the acquisition system, the differential phase between the two antennas is solely a function of the cross-track look angle to the surface reflector (Castelletti and others, 2017; Haynes and others, 2018). Including any of these clutter discrimination

methodologies in radar data processing can enhance the consistency of the interpreted surface reflector.

In contrast to the surface, there is often no a priori insight into bed topography prior to the acquisition and interpretation of radar sounding data. As such, the radargram reprojection and cluttergram simulation approaches cannot be used to discriminate cross-track bed clutter. In this paper, we demonstrate how radar interferometry can be used to produce a consistent interpretation of a glacier bed in areas containing additional ambiguous echoes from cross-track basal reflectors. We are not concerned with demonstrating whether the interpretation of the bed can be shown to be at nadir (ideally with a zero interferometric phase difference between the received echoes, Castelletti and others, 2017; Haynes and others, 2018) as, even for a nadir target, internal acquisition system phase offsets, as well as cross-track surface and subsurface slopes, can introduce a differential phase between the received echoes. For our method, precise correction for these effects is not necessary as we are interested in producing an interpretation of the bed that is consistent within the larger context. This approach can be considered a sparse antenna array version of the array processing methods of Li and others (2012).

The remainder of this paper is structured as follows, after first presenting the fundamentals of radar sounding interferometry we then introduce the dataset on which we have tested our approach. Following this we present the results of our analysis, discuss the larger implications of a consistent bed definition, and finally summarize our main conclusions.

Fundamentals of radar sounding interferometry

Radar sounding interferometry is functionally similar to conventional interferometric SAR only that instead of leveraging the differential phase between two radar measurements acquired at different times to characterize intervening line-of-sight deformation in the surface or to estimate surface elevation, the two radar sounding measurements are contemporaneous (i.e. single-pass interferometry) (Rosen and others, 2000; Reis and others, 2009). A differential phase then relates to a difference in the path length travelled by a reflected echo between a cross-track reflector and two antennas separated by some cross-track distance (the interferometric baseline, L) (Castelletti and others, 2017; Haynes and others, 2018). The two cross-track antennas will henceforth be referred to as 'A' and 'B'.

The problem of cross-track bed clutter is illustrated in Figure 1. Figure 1a presents one position along a transect where both the surface and bed interfaces are flat and no cross-track clutter is generated. Figure 1b then presents a second position along the same transect; however, there is now significant cross-track topography in the ice–bedrock interface adjacent to the point directly below the aircraft. Under such conditions, two echoes could be generated; one from the portion of the interface below the platform (represented by the blue line in Fig. 1b), and one from the preferentially oriented areas on the cross-track topographic slope (the red line in Fig. 1b). These two reflections may be recorded at different times but with similar amplitudes and, without knowledge of the shape of the bed interface, it is not immediately evident which represents a continuation of the reflector observed at a different position along the transect (i.e. Fig. 1a).

Under the conditions presented in Figure 1a, and assuming no internal phase offsets in the electronics of the acquisition system, the phase difference between the bed reflections in the radargrams associated with the A and B antennas is expected to be close to zero. It is important to note though that cross-track slopes in both the surface and bed can lead to non-zero phase differences

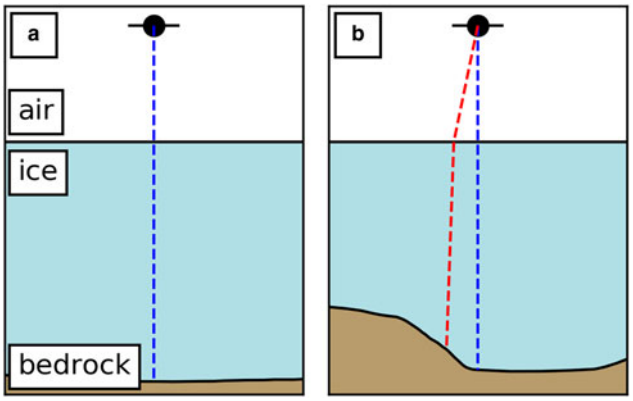

Fig. 1. Two measurement positions along a transect (flight direction is perpendicular to the plane of the page); one (a) with a flat bed interface that does not generate cross-track bed clutter and only a single echo from below the aircraft is recorded (blue line) and a second (b) with significant cross-track bed topography that generates an additional reflection in the form of cross-track bed clutter (red line).

between the A and B radargrams even in the absence of cross-track clutter. In Figure 1b, unless occurring at a phase ambiguity, the reflection from the cross-track slope would present with a different differential phase compared to the reflection from directly below the aircraft. Ambiguity occurs when the differential phase of the cross-track slope reflection is an integer multiple of 2π compared to that from below the aircraft. At this point, even while the reflector is off-nadir, its interferometric phase response is indistinguishable from that of the nadir reflection. Here, assuming each individual reflection in the radargram is the response of a single, continuous target, we argue that by comparing the differential phase of the two reflections (Fig. 1b) with a measure of differential phase in an area of the radargram that is considered free from ambiguous bed clutter (Fig. 1a), the reflection that yields the more consistent interpretation of the bed interface can be identified.

Differential phases between A and B echoes for a particular reflection of interest can be investigated using a roll-corrected interferogram (Ψ_c), as explained below. The uncorrected radar sounding interferogram (Ψ_u) is constructed from the two SAR-focused, single-look complex-valued (SLC), and co-registered A and B radargrams through (Castelletti and others, 2017)

$$\Psi_u = \mathrm{Arg}\left[\frac{1}{nm}\sum_{k=1}^{n}\sum_{h=1}^{m} A(k,\ h)B^*(k,\ h)\right]. \quad (1)$$

Individual pixels in Ψ_u can be considered to be an average of the differential phase values from the A and B radargrams within a moving window. For our analysis, we used a rectangular window that encompassed two sequential fast-time samples (n) across 15 adjacent range lines (m). Range lines were aligned (but not yet co-registered) prior to focusing using known variations in aircraft elevation along the transect.

SAR-focused radargrams are used to build the interferogram as focusing minimizes the along-track beam pattern; isolating clutter to predominantly the cross-track direction. SLC radargrams are required in order to preserve the phase information that is destroyed during incoherent multi-looking (Hélière and others, 2007). Finally, following Castelletti and others (2017), a 1/10-pixel precision co-registration is used to align the two radargrams as finely as possible prior to interferogram creation. Co-registration is accomplished using a constant shift for each pair of range lines.

https://doi.org/10.1017/aog.2020.20 Published online by Cambridge University Press

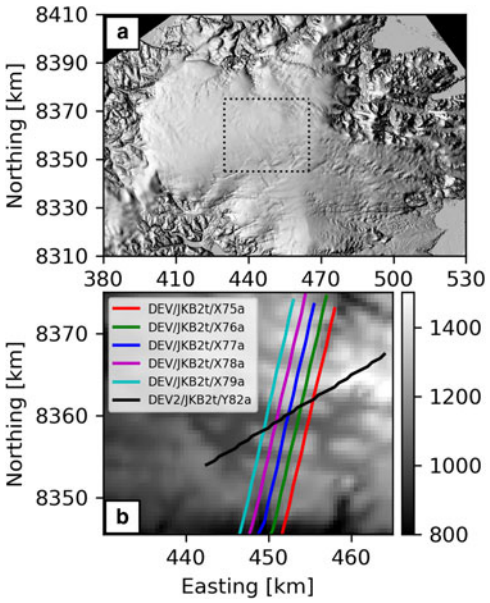

Fig. 2. Overview map of (a) Devon Ice Cap as well as an outline of the area of interest and (b) specific radar transects in the area of interest overlain on a bed topography map corrected for the results of this analysis. All coordinates are presented in UTM zone 17N, bed elevations are presented in meters above sea level.

The correction that must be applied to the differential phases in the uncorrected interferogram (Ψ_u) before individual reflectors can be investigated is due to the roll experienced by the aircraft along the transect (Castelletti and others, 2017). Roll (ϕ) in the acquisition platform is synonymous with a change in look angle (the angle between nadir and the cross-track target) and introduces an additional differential phase (ψ) shift between when a reflection is received by the A and B antennas

$$\psi = \frac{-2\pi L \sin\phi}{\lambda}. \quad (2)$$

L in (2) represents the interferometric baseline (cross-track distance between the A and B antennas) while λ is the wavelength associated with the center frequency of the radar signal. Implicit in (2) is the assumption that expected reflections in the radargrams are the result of nadir surface and subsurface targets. The interferometric roll correction is constant for each range line (change in roll during the collection of an individual range line is negligible) and the roll-corrected interferogram (Ψ_c) is generated by adding the mean roll correction from (2), defined over the same 15-sample window used in (1), to each fast-time sample of the associated range line in the uncorrected interferogram, Ψ_u.

Datasets

The data used in this study were collected in 2018 over Devon Ice Cap (DIC) in the Canadian Arctic (Fig. 2a) as part of a collaborative study between the University of Alberta and the University of Texas Institute for Geophysics (UTIG). Data were collected using UTIG's MARFA acquisition system (Young and others, 2016). MARFA is a dual-phase center version of the HiCARS system (Peters and others, 2007) operating with a 60 MHz center frequency, a 15 MHz signal bandwidth, a 50 MHz pulse sampling frequency and a 19 m interferometric baseline between the antennas. These data are part of a larger investigation into unique subglacial water bodies originally described in Rutishauser and others (2018). Of interest in this study are portions of six transects in the region of the T2 water body located in the low-lying (darkly shaded) trough in the center of Figure 2b (Rutishauser and others, 2018). Figure 2b corresponds to the area within the dashed box overlain on the ArcticDEM (Porter and others, 2019) composite basemap shown in Figure 2a. An updated bed topography model considering the results of this analysis is shown in Figure 2b. The five colored, preferentially north-south, lines (DEV/JKB2t/X75a, DEV/JKB2t/X76a, DEV/JKB2t/X77a, DEV/JKB2t/X78a and DEV/JKB2t/X79a) all cross the trough at an approximate right angle. In contrast, DEV2/JKB2t/Y82a crosses the trough more obliquely.

With the advantage of the consistent bed topography of Figure 2b, it is possible to recognize where bed clutter may manifest along the radargrams (i.e. when flight lines approach steep basal topography at an oblique angle). The most obvious location is along DEV2/JKB2t/Y82a as the aircraft approaches the steep northern slope of the trough. In the center of the trough (between where DEV2/JKB2t/Y82a crosses DEV/JKB2t/X78a and DEV/JKB2t/Y77a), the geometric situation is similar to what is presented in Figure 1a with a limited cross-track topographic variation. However, as cross-track bed topography increases as the aircraft begins to approach the north slope of the trough (a situation similar to what is presented in Fig. 1b), so does the potential to generate cross-track bed clutter.

The portion of the DEV2/JKB2t/Y82a radargram corresponding to the transect in Figure 2b is presented in Figure 3a. The radargram in Figure 3 is the coherent combination of the individual A and B radargrams. The locations where the five DEV/JKB2t/Xxxa intersecting lines cross DEV/JKB2t/Y82a are marked along with the semi-automatically picked surface and bed reflections prior to performing any refinement for potential cross-track bed clutter. The general criteria followed by the human interpreter during the initial horizon picking were to select the first, strongest and most laterally continuous reflection.

The section of the DEV2/JKB2t/Y82a in the vicinity of the northern slope of the main trough highlighted by the dashed box in Figure 3a is reproduced as Figure 3b. Locations where DEV/JKB2t/X77a and DEV/JKB2t/X76a cross DEV2/JKB2t/Y82a are also presented. Four reflections are clearly visible near the northern slope and labeled as features 1 through 4. These features have all been interpreted to be basal in origin due to the absence of rugged surface topography near the summit of DIC (Fig. 2a). However, it is not clear which feature is consistent with the bed reflection in the center of the trough where the T2 lake has been inferred. Initial picking of the bed reflection (black line) followed from the lake reflection, along feature 1 and continued toward the north. The stars represent the position at which the picked DEV/JKB2t/X77a and DEV/JKB2t/76a beds intersect with the DEV2/JKB2t/Y82a radargram. While the Y82a/X76a (northern-most) intersection exhibits little offset between the two interpretations, the Y82a/X77a bed interpretations are significantly different suggesting that these picks may have identified cross-track basal clutter instead of the actual bed.

Results

In order to assess which feature identified in Figure 3b most likely represents the consistent continuation of the lake reflection, we derived the roll-corrected interferogram following the procedure outlined above. Figure 4 presents the interferogram for the same portion of the DEV2/JKB2t/Y82a radargram shown in Figure 3b. The reflections of interest identified in Figure 3b are also highlighted in Figure 4. From the interferogram, the mean differential phase for each feature was estimated and the results are summarized in Table 1.

https://doi.org/10.1017/aog.2020.20 Published online by Cambridge University Press

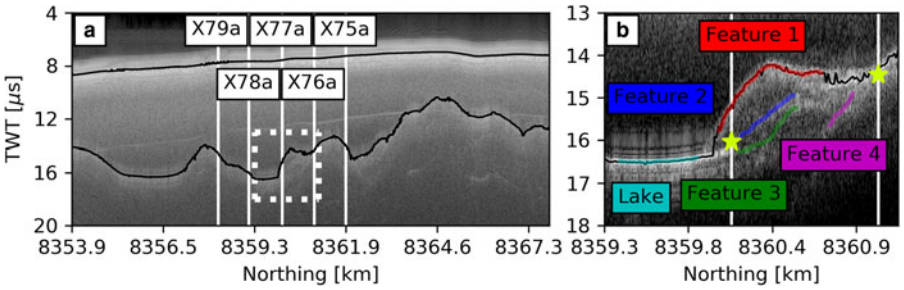

Fig. 3. DEV2/JKB2t/Y82a radargram corresponding to (a) the groundtrack shown in Figure 2b and (b) the immediate vicinity of the northern slope of the main bedrock trough (dashed box in (a)). The positions where the DEV2/JKB2t/Y82a radargram is intersected by the five DEV/JKB2t/Xxxa radargrams are marked in white. Intersecting bed picks from DEV/JKB2t/X77a and DEV/JKB2t/Y76a are highlighted with yellow starts in (b). Black lines correspond to the initial picks for the surface and bed reflections. The unambiguous lake reflection and four features possibly related to cross-track basal clutter are labeled in (b). A different colorbar is used in (b) than in (a) to highlight basal reflections.

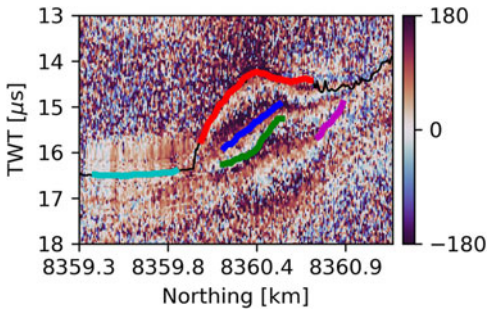

Fig. 4. DEV2/JKB2t/Y82a interferogram in the immediate vicinity of the northern slope of the main bedrock trough. Initial bed picks (black line) and features identified for interferometric testing (cyan, red, blue, green and magenta lines) are highlighted.

Table 1. Summary of mean interferometric phase and standard deviation associated with each feature of interest identified in the DEV2/JKB2t/Y82a radargram

Feature	Mean differential phase Deg	Std dev. Deg
Lake	38.98	29.52
Feature 1	99.34	66.15
Feature 2	115.15	26.69
Feature 3	22.77	82.70
Feature 4	73.41	61.10

The large change in mean differential phase relative to the lake reflection implies that feature 1, the reflection that was initially selected as the representative bed reflection (Fig. 3), is most likely cross-track bed clutter from a situation similar to what is shown in Figure 1b. This interpretation further justified considering the large offset observed between the initial DEV2/JKB2t/Y82a bed interpretation and that of DEV/JKB2t/X77a (Fig. 3b). However, it should be noted that if based solely on the expectation of Gaussian interferometric phase distributions (Castelletti and others, 2017; Haynes and others, 2018), the feature 1 probability density function (as defined by the mean and standard deviation in Table 1) would overlap significantly with that of the lake reflection. Without the near-by intersection with DEV/JKB2t/X77a, statistical methods such as those presented in Castelletti and others (2017) and Haynes and others (2018) would be required to discriminate feature 1 as an off-nadir basal reflection that is inconsistent with that of the lake.

Feature 4 also exhibits a significant difference in mean differential phase relative to the lake reflection and, even though it exhibits a large standard deviation, as it is spatially limited, it is also likely related to cross-track bed clutter. While the bed pick from DEV/JKB2t/X77a more closely matches features 2 and 3, the interferometry results suggest that feature 2 is likely cross-track clutter. This is a result of the large discrepancy in mean differential phase and the fact that the associated Gaussian distributions do not overlap at one standard deviation. Feature 3 exhibits the smallest difference in mean differential phase relative to the lake reflection as well as most overlap with the associated probability density function. It is therefore the feature 3 reflection that is interpreted as the reflection most likely to represent a consistent extension of the bed as it has been defined in the center of the trough.

The interferometry results summarized in Table 1 aid in discriminating the consistent DEV2/JKB2t/Y82a bed reflection (feature 3) from cross-track bed clutter (features 1, 2 and 4). This is supported by a comparison with the bed picks interpreted from the crossing DEV/JKB2t/X77a radargram (Fig. 3b). However, it is worthwhile repeating the analysis process to ensure that the DEV/JKB2t/X77a bed is consistently defined and itself not affected by cross-track bed clutter.

Figure 5a presents the portion of the DEV/JKB2t/X77a radargram corresponding to the transect shown in Figure 2b, while Figure 5b focuses on the northern slope of the main trough. As with Figure 3, the black lines represent the initial interpretation of the surface and bed reflections and the stars represent the points of intersection between the initial (yellow) and interferometry-revised (red) DEV2/JKB2t/Y82a bed picks and the DEV/JKB2t/X77a radargram. A reference reflection in the area of the T2 subglacial lake is selected (labeled again as lake) but unlike Figure 3b, in Figure 5b there is only one reflection in the vicinity of the northern slope (labeled as slope) already suggesting that cross-track bed clutter may not be a significant issue. Figure 6 presents the interferogram associated with the portion of the radargram in Figure 5b. The mean differential phase and standard deviation (in parentheses) associated with the lake (blue) and slope (green) reflections extracted from the interferogram are 24.36° (22.64°) and 26.95° (44.24°), respectively. The very close agreement between the mean differential phases of these two reflectors implies that they represent a consistent bed definition and the initial interpretation of DEV/JKB2t/X77a is unaffected by cross-track basal clutter.

Discussion

The results of our analysis have shown radar sounding interferometry is capable of discriminating basal clutter, leading to a more consistent interpretation of the bed. While demonstrating this technique is the goal of this study, it is also useful to examine how subsequent analyses based on the bed interpretation can be affected by cross-track basal clutter.

Figure 7a presents the central portion of the DEV2/JKB2t/Y82a radargram across the main trough containing the T2 water body and the final interpretations of both the surface and the bed (solid black lines). The dashed black line represents the original interpretation of the bed prior to adjusting for basal clutter. At its maximum, there is approximately a 2 μs two-way travel time difference between the original and revised bed reflection as determined from interferometry. For a representative relative dielectric permittivity of ice (E_r equal to 3.15), this

https://doi.org/10.1017/aog.2020.20 Published online by Cambridge University Press

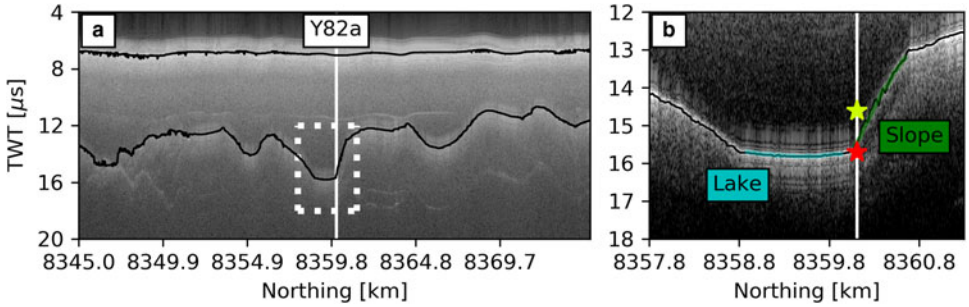

Fig. 5. DEV/JKB2t/X77a radargram corresponding to (a) the groundtrack shown in Figure 2b and (b) the immediate vicinity of the northern slope of the main bedrock trough (dashed box in (a)). The position where the DEV/JKB2t/X77a radargram is intersected by the DEV2/JKB2t/Y82a radargram is marked. Original and interferometry-revised intersecting bed pick from DEV2/JKB2t/Y82a are highlighted with yellow and red stars, respectively, in (b). Black lines correspond to the initial manual picks for the surface and bed reflections. The unambiguous lake reflection and the northern slope reflection are labeled in (b). A different colorbar is used in (b) than in (a) to highlight basal reflections.

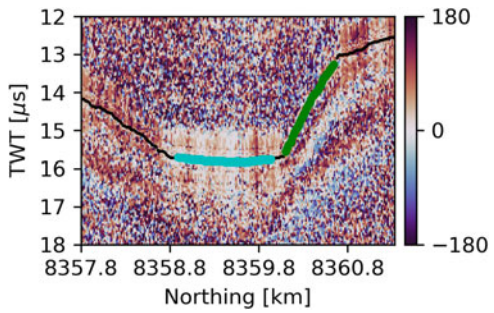

Fig. 6. DEV/JKB2t/X77a interferogram in the immediate vicinity of the northern slope of the main bedrock trough. Initial bed picks (black line) and lake and slope features identified for interferometric testing are highlighted.

corresponds to a change of 168 m in the elevation of the bed; approximately one-quarter of the total ice thickness in the T2 trough.

Carrying this analysis further, Figure 7b presents the subglacial hydraulic head derived from the ice surface and the two interpretations of the bed (solid and dashed black lines) following Shreve (1972); Rutishauser and others (2018). The change in the hydraulic head after accounting for basal clutter (original minus revised) is also shown. Not only does the hydraulic head drop by almost 30 m in the region containing previously ambiguous basal clutter, there is also a significant change in the hydraulic head gradient. The slope in the hydraulic head is important in water routing models as it determines where water flows (down hydraulic gradients) and where it can pool (in the areas of near-zero hydraulic gradient, potentially forming subglacial lakes). In the original interpretation of the bed, the hydraulic gradient suggested water could potentially pond at the top of the trough's northern slope wall (between 8360.5 and 8360.8 km in Fig. 7b). In the revised bed interpretation, this area of potential ponding has been dramatically reduced, suggesting liquid water flowing along the bed from the north will preferentially concentrate in the base of the trough.

Finally, the revised interpretation of the bed reflection has significant implications for the possible extent of the lake occupying the trough (Rutishauser and others, 2018). Careful inspection of Figure 3b shows that the original DEV2/JKB2t/Y82a bed interpretation began to follow feature 1 before the strong, lower-relief bed echo it was following along the base of the trough ended (approximately at the intersection with the DEV/JKB2t/X77a transect). Subsequent analysis may suggest that this strong reflection omitted in the original interpretation of DEV2/JKB2t/Y82a bed exhibits reflectivities high enough to indicate the presence of liquid water (Rutishauser and others, 2018). Lake boundaries based on the original interpretation of the bed would have then underrepresented the size of the water body.

While this study demonstrates how relative differences in interferometric phase can be leveraged in order to define the most consistent bed reflection, it is worthwhile to revisit the absolute interferometric phase angles; specifically, those related to the lake reflections (Figs 3b and 5b). The interferometric phase and standard deviation (in parentheses) of the lake reflection as extracted from the DEV2/JKB2t/Y82a and DEV/JKB2t/X77a interferograms (Figs 4 and 6) are 38.98° (29.52°) and 24.36° (22.64°), respectively. It is clear that neither lake reflection exhibits the typical interferometric response that would be associated with a flat, specular target at nadir (i.e. 0° mean differential phase). Internal, systematic phase offsets between the A and B antennas within the MARFA acquisition system are expected to be on the order of single digits of degrees and unable to completely account for the observed absolute phase differences.

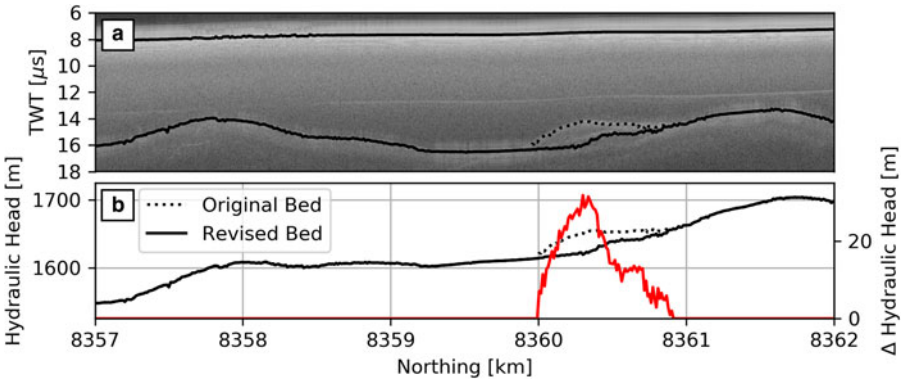

Fig. 7. Central portion of the DEV2/JKB2t/Y82a radargram (a) and the associated absolute (black) and change in (red) hydraulic head profiles (b) derived from the interpreted surface and bed picks. Solid black lines refer to the revised interferometry-corrected interpretation of the bed reflection. The black dashed line shows the original interpretation of the bed.

https://doi.org/10.1017/aog.2020.20 Published online by Cambridge University Press

The most likely source of the differential phases observed in the lake reflections is related to the presence of cross-track slopes. Cross-track slopes introduce slight changes in the length of the radar propagation paths between A and B antennas and their respective points of reflection on the lake surface compared to a situation where both the ice and lake surfaces are flat (similar to Fig. 1a). These differences in path length then result in the phase offsets between the basal/lake surface reflections recorded by both the A and B antennas. As cross-track slopes at both the ice and lake surfaces introduce variations in radar path lengths, their respective contributions cannot be separated without considering additional sources of information (such as a surface digital terrain model).

Conclusions

Cross-track clutter represents a source of ambiguity and impediment in the consistent interpretation of surface and bed horizons from SAR-focused radar sounding data. Surface clutter in a radargram can be discriminated through either interferometry or by relying on available surface DEMs. In contrast, as there is often no a priori knowledge of bed topography prior to radargram interpretation, similar DEM-reliant techniques cannot be used to discriminate clutter due to cross-track bed topography. In this study, we demonstrate that interferometry can successfully discriminate basal clutter and be used to produce a continuous interpretation of the bed that is consistent with regions unaffected by clutter. Furthermore, we have shown that effectively accounting for cross-track clutter can have significant implications on derived ice thicknesses, basal water routing models and subglacial water body extents.

Acknowledgement. We thank The W. Garfield Weston Foundation who funded the aero-geophysical survey over Devon Ice Cap and subsequent standard data processing, The G. Unger Vetlesen Foundation who funded the subsequent interferometric data processing, and the UTIG Postdoctoral Fellowship program. We also thank the Polar Continental Shelf Program, Kenn Borek Air Ltd. and the field team for their excellent support, and NRI and the peoples of Grise Fjord and Resolute Bay for permission to conduct airborne surveys over Devon Ice Cap. This is UTIG contribution number 3650.

References

Bingham RG and Siegert MJ (2007) Radio-echo sounding over polar ice masses. *Journal of Environmental and Engineering Geophysics* **12**(1), 47–62 (doi: 10.2113/JEEG12.1.47).

Castelletti D and 9 others (2017) An interferometric approach to cross-track clutter detection in two-channel VHF radar sounders. *IEEE Transactions of Geoscience and Remote Sensing* **55**(11), 6128–6140 (doi: 10.1109/TGRS.2017.2721433).

Haynes MS, Chapin E, Moussessian A and Madsen SN (2018) Surface clutter discrimination analysis for radar sounding interferometry. *IEEE Transactions on Aerospace and Electronic Systems* **55**(2), 989–1003 (doi: 10.1109/TAES.2018.2867689).

Hélière F, Lin C-C, Corr H and Vaughn D (2007) Radio echo sounding of pine island glacier, West Antarctica: aperture synthesis processing and analysis of feasibility from space. *IEEE Transactions of Geoscience and Remote Sensing* **45**(8), 2573–2582 (doi: 10.1109/TGRS.2007.897433).

Holt JW, Peters ME, Kempf SD, Morse DL and Blankenship DD (2006) Echo source discrimination in single-pass airborne radar sounding data from the Dry Valleys, Antarctica: implications for orbital sounding of Mars. *Journal of Geophysical Research* **111**(E06S24), 1–13 (doi: 10.1029/2005JE002525).

Legarsky JL, Gogineni SP and Akins TL (2001) Focused synthetic aperture radar processing of ice-sounder data collected over the Greenland ice sheet. *IEEE Transactions of Geoscience and Remote Sensing* **39**(10), 2109–2117 (doi: 10.1109/36.957274).

Leuschen CS, Gogineni SP and Tammana D (2000) SAR processing of radar echo sounder data. In *IGARSS 2000 IEEE 2000 International Geoscience and Remote Sensing Symposium. Taking the Pulse of the Planet: The Role of Remote Sensing in Mapping the Environment. Proceedings (Cat. No. 00CH37120)*, 24–28 July 2000, Vol. 6, IEEE, Honolulu USA, 2570–2572 (doi: 10.1109/IGARSS.2000.857863).

Li J and 8 others (2012) High-altitude radar measurements of ice thickness over the Antarctic and Greenland ice sheets as a part of operation IceBridge. *IEEE Transactions of Geoscience and Remote Sensing* **51**(2), 742–754 (doi: 10.1109/TGRS.2012.2203822).

Peters ME and 5 others (2007) Along-track focusing of airborne radar sounding data from West Antarctica for improving basal reflection analysis and layer detection. *IEEE Transactions of Geoscience and Remote Sensing* **45**(9), 2725–2736 (doi: 10.1109/TGRS.2007.897416).

Peters ME, Blankenship DD and Morse DL (2005) Analysis techniques for coherent airborne radar sounding: application to West Antarctic ice streams. *Journal of Geophysical Research* **110**(B06303), 1–17 (doi: 10.1029/2004JB003222).

Porter C and 28 others (2019) ArcticDEM. [Online]. Available at https://www.pgc.umn.edu/data/arcticdem/.

Reis JJ, Hensley S, Willams MA and Woods D (2009) Updating GeoSAR for full-pol interferometric capability. In *2009 IEEE Radar Conference*, 4–8 May 2009, IEEE, Pasadena USA (doi: 10.1109/RADAR.2009.4977082).

Robin G de Q (1975) Radio-echo sounding: geological interpretations and applications. *Journal of Glaciology* **15**(73), 49–64 (doi: 10.3189/S0022143000034262).

Rosen PA and 6 others (2000) Synthetic aperture radar interferometry. *Proceedings of the IEEE* **88**(3), 333–382 (doi: 10.1109/5.838084).

Rutishauser A and 8 others (2018) Discovery of a hypersaline subglacial lake complex beneath Devon Ice Cap, Canadian Arctic. *Science Advances* **4**(4), 1–6 (doi: 10.1126/sciadv.aar4353).

Shabtaie S and Bentley CR (1988) Ice-thickness map of the West Antarctic ice streams by radar sounding. *Annals of Glaciology* **11**, 126–136 (doi: 10.3189/S0260305500006443).

Shreve RL (1972) Movement of water in glaciers. *Journal of Glaciology* **11**(62), 205–214 (doi: 10.3189/S002214300002219X).

Wright A and Siegert M (2012) A fourth inventory of Antarctic subglacial lakes. *Antarctic Science* **24**(6), 659–664 (doi: 10.1017/S095410201200048X).

Young DA, Schroeder DM, Blankenship DD, Kempf SD and Quartini E (2016) The distribution of basal water between Antarctic subglacial lakes from radar sounding. *Philosophical Transactions of the Royal Society A* **374**, 1–21 (doi: 10.1098/rsta.2014.0297).